Nuclear Physics B77 (1974) 1–34. North-Holland Publishing Company

DIFFRACTION DISSOCIATION AND COULOMB DISSOCIATION OF HIGH-ENERGY NEUTRONS BY NUCLEI*

D.D. O'BRIEN**, M.J. LONGO and J.C. VANDERVELDE
University of Michigan, Ann Arbor, Michigan 48104

M.B. DAVIS*** and M.N. KREISLER‡
Princeton University, Princeton, New Jersey 08540

Received 12 November 1973

Abstract: We present the results of a spark chamber experiment in which we studied the reaction

$n + A \to (p + \pi^-) + A'$,

where the $(p\pi^-)$ pair is coherently produced off carbon, copper, and lead nuclei. Between 5 000 and 55 000 good events were collected with each target. Incident neutrons in the momentum range 10 to 28 GeV/c were used. Forward-going $(p\pi^-)$ pairs from the above reaction were detected in a wire spark chamber spectrometer which measured the momentum and angles of each particle. The observation of a sharp forward peak (of width appropriate to the nuclear radius) indicated that a large fraction of the events were coherently produced. There is no evidence for any appreciable production of the well-established $I = \frac{1}{2}$ nucleon isobars; our limits appear to be inconsistent with estimates based on a straightforward extrapolation of pp data. The lead data show evidence for coulomb production of the $\Delta(1236)$. The carbon data indicate a spin $J \geqslant \frac{3}{2}$ for the coherently produced $(p\pi^-)$ states with pure $J = \frac{3}{2}$ possible. We cannot draw any firm conclusions about helicity conservation. The Drell-Hiida-Deck model does not adequately fit the data, nor is the double-Regge-pole model completely satisfactory.

1. Introduction

In this article we describe an experiment in which we studied the reaction

$$n + A \to (p + \pi^-) + A', \tag{1}$$

where the incident neutron dissociates into a $(p\pi^-)$ pair in scattering coherently off

* Work supported by the US National Science Foundation Grant GP27394 and the US Atomic Energy Commission.
** Now at Physics Department, McGill University, Montreal, Quebec, Canada.
*** Now at Carnegie Institution of Washington, Department of Terrestrial Magnetism, Washington, D.C. 20015.
‡ Now at Department of Physics and Astronomy, University of Massachusetts, Amherst, Massachusetts 01002.

a nucleus A. The experiment is of particular interest, in part because this process has not previously been studied*. This reaction can proceed either through the strong interaction or, particularly for high Z nuclei, through the coulomb interaction. It was hoped that the two modes of interaction could be distinguished by examining the Z dependence of the invariant mass distribution of the coherently produced $(p\pi^-)$ pairs. We also wished to determine whether the $(p\pi^-)$ mass distributions exhibited any peaks which would correspond to resonance production. Most experiments which have studied processes similar to reaction (1) have observed what has been interpreted as resonance production [3, 4]. However, most of these experiments were done with free nucleons as targets, usually at rather large momentum transfers, and often with limited statistical accuracy. Our data for nuclei, on the other hand, is restricted to low t, and only isospin $\frac{1}{2}$ final states are important.

2. Theoretical preliminary

Reviews of the properties of diffraction dissociation and coulomb dissociation, together with discussions of the results of experiments that have studied these processes, can be found in refs. [4–7]. Some of the early theoretical work in this field can be found in refs. [8–10].

In a diffractive process the incident particle scatters coherently on a target nucleus that remains intact and in the ground state or in some other well-defined excited state. A consequence of this coherence is that diffraction dissociation, like elastic scattering, is characterized by a sharp peak at small t', where t' is the square of the four-momentum transfer minus its minimum value,

$$t' \equiv t - t_{\min} \,. \tag{2}$$

Here $t_{\min}$ is given by

$$t_{\min} \cong -\tfrac{1}{4}[(M_{p\pi}^2 - M_n^2)/P_n]^2 \,, \tag{3}$$

where $M_{p\pi}$ is the invariant mass of the diffractively produced $(p\pi^-)$ system, M_n is the rest mass of the beam neutron, and P_n is the momentum of the neutron. To a good approximation**

$$t' \simeq P_\perp^2 \,, \tag{2'}$$

where $P_\perp$ is the transverse component of the three-momentum transferred to the target nucleus. The width of the sharp forward peak is determined by the size of the target nucleus. The peak is expected to fall off like $e^{-b|t'|}$ where

$$b \simeq 10.8\, A^{\frac{2}{3}}\,(\mathrm{GeV}/c)^{-2} \,.$$

* Brief reports of some of the results of this experiment were published in ref. [1]. A more detailed report is given in ref. [2].

** Eqs. (2′) and (3) are correct to within 1% for this experiment.

If reaction (1) proceeds coherently through the strong interaction, for isospin zero nuclei the $(p\pi^-)$ system must have $I = \frac{1}{2}$, but there is no restriction on its spin J. If the $(p\pi^-)$ system is a pure state with $J = \frac{1}{2}$ and definite parity, the decay angular distribution in the $(p\pi^-)$ c.m. must be isotropic in both the helicity and Gottfried-Jackson frames of reference. At $t' = 0$ a pure state with $J = \frac{3}{2}$ and definite parity would have decay angular distributions in both frames proportional to $(1 + 3\cos^2\theta_\pi^*)$ where θ_π^* is the polar angle of the π^- [11]. For larger J the peaks in the angular distributions become steeper and the minimum becomes broader and flatter [12].

For reaction (1) helicity conservation in the t-channel (s-channel) over a given t' interval implies that the decay angular distribution in $\cos\theta^*$ is independent of t' in the Gottfried-Jackson (helicity) frame of reference provided that a pure J^P state is produced or that the various amplitudes in a mixed state have the same t' dependence. Helicity conservation in the t-channel (s-channel) also implies a flat azimuthal angular distribution in the Gottfried-Jackson (helicity) frame of reference, regardless of the purity of the produced state [13].

We now discuss briefly the properties of coulomb dissociation [4, 5, 8, 10]. In coherent coulomb dissociation, the incident neutron dissociates into the $(p\pi^-)$ system by interaction with the coulomb field of the target nucleus. As in diffraction dissociation, the nucleus remains intact and in some well-defined energy state. At high energies most of the coulomb production occurs outside of the target nucleus, and the forward peak in the t' distribution should be steeper than in diffraction dissociation for the same target nucleus. The production cross section of coulomb dissociated states is expected to vary approximately as Z^2. Because the exchanged particle is the photon, the isotopic spin of the coulomb produced $(p\pi^-)$ system can be different from that of the incident neutron.

3. Experimental apparatus

3.1. The neutron beam

A general layout of the neutron beam is shown in fig. 1. The neutron beam was taken off at 0° from an 18 cm long beryllium target in the slow extracted proton beam of the Brookhaven AGS. Proton beam momenta of 21 GeV/c and 28.5 GeV/c were used. The observed momentum distribution of the coherently produced $(p\pi^-)$ systems off carbon at the higher proton momentum is shown in fig. 2. Assuming that the production cross section is approximately energy independent [3, 4, 7], fig. 2 represents rather well the general shape of the neutron spectrum above 10 GeV/c.

Charged particles were removed from the neutron beam by two sweeping magnets located upstream of the defining collimator and a sweeping magnet and a pitching magnet both located downstream of the collimator. The sweeping magnets

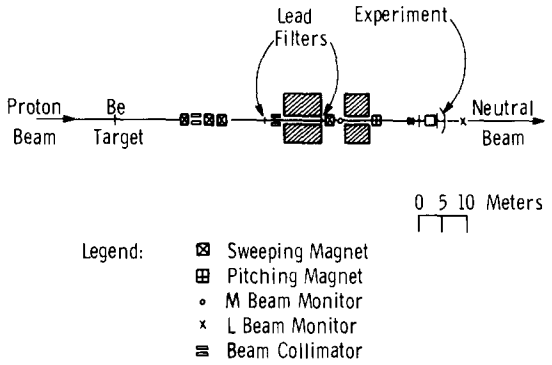

Fig. 1. General beam layout. Transverse dimensions are exaggerated for clarity.

deflected charged particles horizontally. Lead filters, each about 3 radiation lengths thick, were placed just ahead of each sweeping magnet to remove gammas in the beam. The pitching magnet deflected charged particles (formed in the air and a beam monitor down-stream of the sweeping magnets) vertically away from the apparatus.

At the exit of the pitching magnet, the neutron beam was approximately 2.5 cm in diameter with negligible halo. Two monitor telescopes, denoted as L and M monitors in fig. 1, were placed in the neutron beam to measure relative intensity. Each

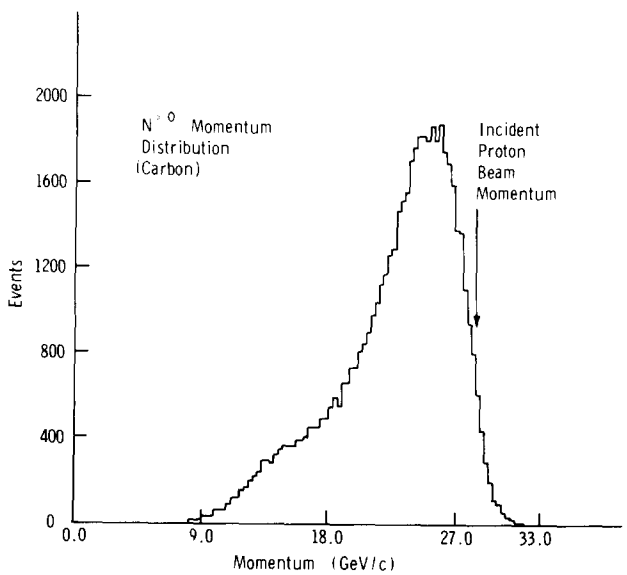

Fig. 2. Momentum distribution of the $(p\pi^-)$ system for $|t'| < 0.02$ $(\mathrm{GeV}/c)^2$ and a proton beam momentum of 28.5 GeV/c. The geometrical efficiency of the apparatus, which varies slowly with momentum, has not been unfolded.

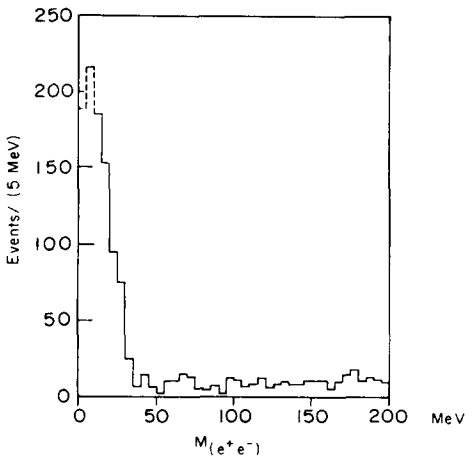

Fig. 3. Invariant mass $M_{e^+e^-}$ for lead data. The data have not been corrected for a bias against small opening angles.

monitor consisted of three counters. The first counter was an anticounter which was followed by a 1.28 cm lucite converter. The second and third counters were in coincidence and detected charged particles produced in the converter.

The K_L^o contamination in the neutron beam was estimated by looking for various K^o decay modes that could contribute to our data. The data were checked for $K^o \to \pi^+ + \pi^-$ contamination by reconstructing the pairs of tracks of the good events assuming that they were due to a $(\pi^+\pi^-)$ pair. No evidence of this decay was found in our data. The data were also checked for any evidence of kaons decaying *via* the process $K_L^o \to \pi^+ + \pi^- + \pi^o$ using a kinematic trick that differentiates this process from other three-body decays [14]. We found no evidence of this decay mode in our data. We also estimated the K_L^o contamination in the neutron beam from production data for charged kaons by high-energy protons. From this we estimate the K_L^o contamination is $\lesssim 0.5\%$ for kaon momenta > 16 GeV/c [15].

Despite the use of lead converters in the neutron beam, a small gamma ray contamination remained in the beam. This was apparent when the data for the lead target were reconstructed with the hypothesis that the events were (e^+e^-) pairs. Fig. 3 shows the invariant mass distribution for a sample of the lead data. The narrow peak at small masses is due to pair production by the small contamination of γ's in the beam. Its width is consistent with that expected from the resolution of the spectrometer and coulomb scattering in the lead*. It was found that essentially all the γ's had momenta < 20 GeV/c in the higher energy beam and < 15 GeV/c for the lower energy beam. Cuts were therefore applied to the data for pairs of

* There is a strong bias against "small" (e^+e^-) masses. In order for an event to be successfully reconstructed, it was necessary that two sparks be found in the second pair of chambers (subsect. 4.1). The opening angle of the (e^+e^-) pairs is so small that the sparks in the second pair of chambers were often too close together to be resolved. The data in fig. 3 have not been corrected for this effect.

tracks whose total momentum was less than 20 GeV/c and 15 GeV/c respectively. The remaining contamination had a negligible effect on the $(p\pi^-)$ mass distributions. The (e^+e^-) pairs provided a useful check on the mass resolution of the apparatus (subsect 3.3).

3.2. Wire chamber spectrometer and target assembly

The layout of the experimental apparatus is shown in fig. 4. A detailed drawing of the target assembly is shown in fig. 5. The target was surrounded by an almost complete anticounter shield. There was an aperture on the downstream side of the anticounter box of width 8.8 cm and of height 7.3 cm that was covered by the trigger counter P_1. Data were taken primarily with 1.25 cm carbon, 0.132 cm copper, and 0.168 and 0.201 cm lead targets.

The wire spark-chamber spectrometer was symmetrically placed in the beam downstream of the target as shown in fig. 4. The trigger requirement, $P_1 L_2 R_2 \bar{A}$ or $P_1 L_3 R_3 \bar{A}$, was kept simple to facilitate efficiency calculations. The anticounters, designated by $\bar{A}$ in the trigger requirement, consisted of the anticounter box (A_9) surrounding the target, the anticounter (A_0) located on the upstream side of the anticounter box, an array of anticounters (A_1 through A_6) surrounding the upstream aperture of the spectrometer magnet, and two anticounters (A_7 and A_8)

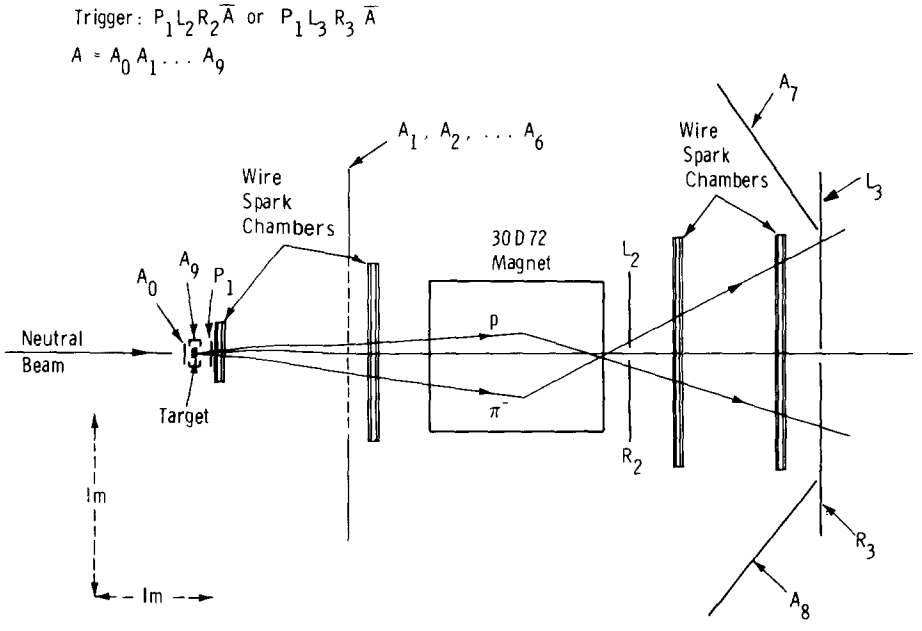

Fig. 4. Plan of experiment. Note different scales.

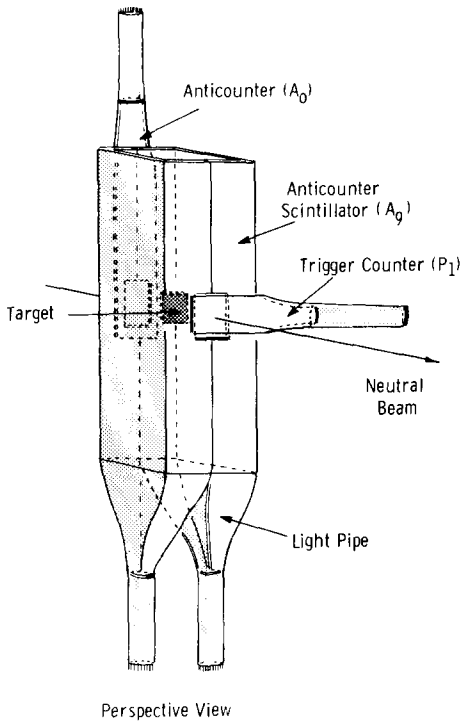

Fig. 5. Target assembly and anticounter box.

downstream of the last wire chamber. Lead plates of 0.64 cm thickness were placed before the anticounters $A_1, A_2, \ldots, A_6$ to convert γ's.

A magnet with 76.2 cm wide and 182.9 cm long rectangular pole face and 15.24 cm high rectangular aperture was used. The magnetic field, measured by the magnet measurement group of the AGS and by us, was determined with an uncertainty of less than 0.5%. The central field values of the magnet for data accumulation at the proton beam momenta of 21 GeV/c and 28.5 GeV/c were 13.9 kg and 18.0 kG respectively. Eight wire spark chambers with magnetostrictive readout were used in the spectrometer. The spark chambers were arranged in pairs with one chamber having horizontal and vertical wires and the other having wires at $\pm 45^\circ$ to the vertical. The rotated chambers were necessary to resolve the ambiguity in track coordinates resulting from the fact that two particles, a proton and pion, were detected in each chamber. Two pairs of chambers were located upstream of the magnet and two pairs downstream of the magnet.

Helium bags were placed between the spark chambers on the upstream and downstream sides of the spectrometer magnet to minimize the multiple scattering of the proton and the pion. Sheets of 0.95 cm thick soft iron had to be placed over the magnetostrictive wires of the four spark chambers closest to the magnet to

shield the wires from fringe fields ~ 100 Gauss. It had been found that without this shielding, the pulses from the magnetostrictive wands were affected by the magnetic field.

3.3. Acceptance and resolution of the spectrometer

The acceptance of the spectrometer was determined by a straightforward Monte-Carlo calculation. Fig. 6 shows a typical distribution of the acceptance as a function of $\cos\theta_\pi^*$, the cosine of the pion angle relative to the direction of the incident neutron in the $(p\pi^-)$ center-of-mass frame of reference, for the ranges of the variables shown in the figure. It should be noticed that the experiment is strongly biased against backward pions in the $(p\pi^-)$ center-of-mass system. The apparatus is also biased against very small invariant $(p\pi^-)$ masses at low incident neutron momenta, but at high momenta small invariant $(p\pi^-)$ masses are favored for all ranges of t'. The acceptance as a function of t', determined from Monte-Carlo calculations for $M_{(p\pi^-)} = 1.4$ GeV and $P_{(p\pi^-)} = 26$ GeV/c, is shown in fig. 7. For events with $-t' \leqslant 0.03$ (GeV/c)^2 the cosine of the pion angle ($\cos\theta_\pi^*$) in the $(p\pi^-)$ center-of-mass frame of reference was randomly generated according to the distribution $(1 + 3\cos^2\theta_\pi^*)$ because in this range of t this function adequately fits our experimental results [1, 2]. For events with $-t' > 0.03$ (GeV/c)^2, $\cos\theta_\pi^*$ was uniformly generated over the interval $-1 \leqslant \cos\theta_\pi^* \leqslant 1$. From fig. 7 it is seen that the acceptance is roughly independent of t' over the interval $0 \leqslant |t'| \leqslant 0.05$ (GeV/c)^2.

Because $t' \simeq -P_\perp^2$ the errors in t' are determined by the errors in $P_\perp$, the transverse momentum of the $(p\pi^-)$ system. The measurement error in t' is approximately given by

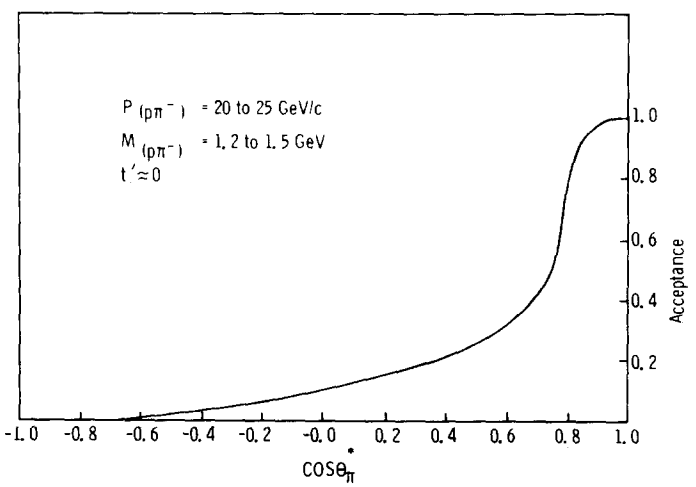

Fig. 6. Typical acceptance versus $\cos\theta_\pi^*$.

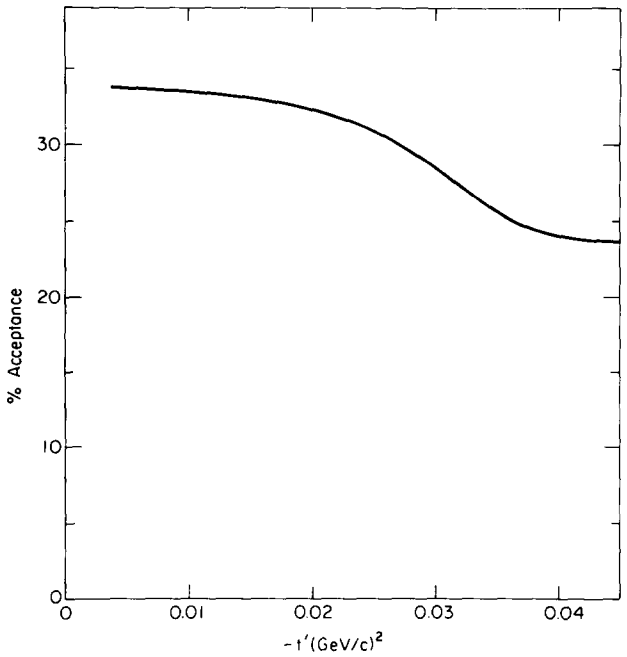

Fig. 7. Typical acceptance *versus* $-t'$. A $(1 + 3\cos^2\theta_\pi^*)$ distribution was assumed for $|t'| \leqslant 0.03$ and a flat distribution in θ_π^* for $|t'| > 0.03$.

$$\mathrm{d}t' \simeq -2P_\perp \mathrm{d}P_\perp$$

$$\simeq -2P_\perp \{P_\mathrm{p}^2 \mathrm{d}\theta_\mathrm{p}^2 + P_\pi^2 \mathrm{d}\theta_\pi^2 + \theta_\mathrm{p}^2 \mathrm{d}P_\mathrm{p}^2 + \theta_\pi^2 \mathrm{d}P_\pi^2\}^{\frac{1}{2}} . \tag{4}$$

The subscripts p and π refer to the proton and pion respectively. For our experiment, the $P\mathrm{d}\theta$ terms generally dominate the $\theta \mathrm{d}P$ terms. The momentum resolution for the proton (pion) is given by

$$\frac{\mathrm{d}P}{P} \cong \frac{P\,\mathrm{d}\theta_\mathrm{B}}{1.2\,BL_\mathrm{eff}}, \tag{5}$$

where P is in units of GeV/c, BL_eff is the value of the integral of $\boldsymbol{B}\cdot \mathrm{d}\boldsymbol{l}$ through the center of the spectrometer magnet† and $\mathrm{d}\theta_\mathrm{B}$ is the uncertainty in the bending angle determination given by

$$(\mathrm{d}\theta_\mathrm{B})^2 = [\mathrm{d}\theta_\mathrm{meas}^2 + \mathrm{d}\theta_\mathrm{ms}^2]_\mathrm{upstrm} + [\mathrm{d}\theta_\mathrm{meas}^2 + \mathrm{d}\theta_\mathrm{ms}^2]_\mathrm{dwstrm}, \tag{6}$$

where $\mathrm{d}\theta_\mathrm{meas}$ is the measurement error and $\mathrm{d}\theta_\mathrm{ms}$ is the uncertainty due to multiple

† BL_eff was 36.0 kG · m for the data taken with an 18.0 kG central field.

Table 1
Angular and momentum resolution [a)]

Particle momentum (GeV/c)	$d\theta_B$ (mr)	$d\theta$ (mr) [b)]	$Pd\theta$ (GeV/c)	dP/P (%)
5	$\pm$ 1.32	$\pm$ 1.86	$\pm$ 9.3×10^{-3}	$\pm$ 0.15
10	1.26	1.11	11.1×10^{-3}	0.29
15	1.25	0.91	13.6×10^{-3}	0.44
20	1.25	0.82	16.5×10^{-3}	0.58
25	1.25	0.78	19.5×10^{-3}	0.72
30	1.25	0.76	22.7×10^{-3}	0.87

a) A lead target with a thickness of 0.185 cm is assumed; thicknesses of 0.168 cm and 0.201 cm were used for data taking. The angular resolutions and mass resolution is somewhat better for carbon and copper targets.
b) $d\theta$ is due to multiple coulomb scattering in the target and to the spark chamber resolution

scattering in the region upstream (downstream) of the bending magnet. The uncertainty in angular measurement $d\theta_{meas}$ is determined by dividing the wire chamber resolution ($\simeq 0.7$ mm) by the distance between the first and second pairs of wire chambers upstream (downstream) of the spectrometer magnet.

Because the lab angles are small in the diffraction process (1), the θdP terms in eq. (4) can be calculated with the formula

$$\theta dP = \theta P\left(\frac{dP}{P}\right) \simeq P^* \sin\theta^* \left(\frac{dP}{P}\right), \tag{7}$$

where we have assumed that $P^* \sin\theta^* \simeq P\theta$. (The superscript* refers to the $(p\pi^-)$ center-of-mass frame.) The $d\theta_p$ and $d\theta_\pi$ terms in eq. (4) can be calculated in a manner similar to $d\theta_B$.

In table 1 we list the various uncertainties for six different particle momenta passing through the spectrometer magnet. The values of $d\theta$ were calculated for a lead target with a thickness intermediate between the two thicknesses actually used. For $P = 10$ GeV/c we get $d\theta \simeq 1$ mr and $dP/P \simeq 0.3\%$.

The resolution in t' calculated with eq. (4) is given in table 2. For this table a lead target was assumed and typical values of 10 GeV/c and 15 GeV/c were used for the pion and proton momenta respectively. We note from eq. (4) that $dt' \propto |t'|^{\frac{1}{2}}$. A direct check on the t' resolution is discussed in subsect 5.2.

The mass resolution of the experiment can be expressed in terms of the angular and momentum resolutions of the pion and the proton. The invariant mass of the $(p\pi^-)$ system is given by

$$M^2_{(p\pi^-)} = (E_p + E_\pi)^2 - (P_p + P_\pi)^2 . \tag{8}$$

It can be shown that if the opening angle of the proton-pion pair, $\theta_{p\pi}$, is small (for

Table 2
t' resolution in units of $(\mathrm{GeV}/c)^2$ for typical pion and proton momenta and a lead target.

	$M_{p\pi^-}$ = 1.2 GeV		$M_{p\pi^-}$ = 1.45 GeV		$M_{p\pi^-}$ = 1.7 GeV	
$\sin\theta^*_\pi$	0.6	1.0	0.6	1.0	0.6	1.0
$-t'((\mathrm{GeV}/c)^2)$						
0.001	$\pm 1.11 \times 10^{-3}$	$\pm 1.11 \times 10^{-3}$	$\pm 1.11 \times 10^{-3}$	$\pm 1.12 \times 10^{-3}$	$\pm 1.12 \times 10^{-3}$	$\pm 1.13 \times 10^{-3}$
0.005	2.48	2.49	2.49	2.50	2.49	2.52
0.010	3.51	3.51	3.52	3.53	3.52	3.56
0.020	4.97	4.97	4.98	5.00	4.99	5.04
0.030	6.08	6.09	6.09	6.12	6.11	6.17
0.040	7.02	7.03	7.04	7.07	7.06	7.12

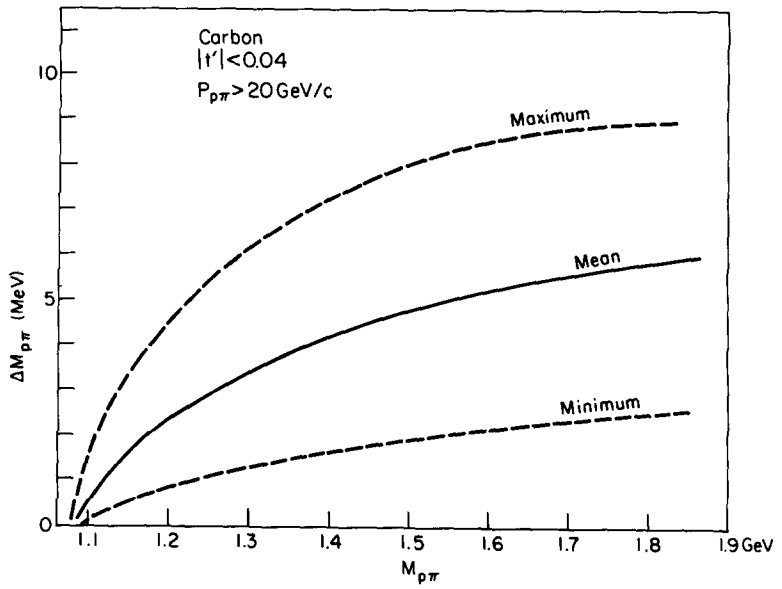

Fig. 8. Calculated mass resolution for carbon data at the higher proton beam energy for $|t'| < 0.04$ (GeV/c)^2. For a given event, $\Delta M_{p\pi}$ depends on how the momentum is shared between the pion and proton. Upper and lower limits for our geometry are shown.

this experiment $\theta_{p\pi}$ is generally $< 5°$), the mass resolution $\Delta M_{(p\pi^-)}$ is given by [2]

$$\Delta M_{(p\pi^-)} \simeq \frac{1}{2M_{p\pi^-}} \left\{ d\theta^2_{p\pi} (2\theta_{p\pi} P_p P_\pi)^2 + dP^2_p \left(P_\pi \theta^2_{p\pi} + \frac{M^2_\pi}{P_\pi} - \frac{M^2_p P_\pi}{P^2_p} \right)^2 \right.$$

$$\left. + dP^2_\pi \left(P_p \theta^2_{p\pi} + \frac{M^2_p}{P_p} - \frac{M^2_\pi P_p}{P^2_\pi} \right)^2 \right\}^{\frac{1}{2}}, \qquad (9)$$

where M_p and M_π are respectively the rest masses of the proton and pion. Fig. 8 shows the calculated values of $\Delta M_{(p\pi^-)}$ for the higher energy carbon data for $|t'| < 0.04$ (GeV/c)^2. Note that for $M_{p\pi} \simeq 1.35$ GeV, the mass resolution is $\lesssim 5$ MeV.

The gamma ray contamination in the lead data provided a check on our calculations of the mass resolution. The true opening angles of the (e^+e^-) pairs produced by gamma rays in the lead target can be taken as zero for our purposes. Fig. 9 shows the measured opening angle distribution of charged pairs from the lead target for $|t'| < 0.01$ (GeV/c)^2, $P_{(e^+e^-)} < 18$ GeV/c. The distribution is determined primarily by coulomb scattering and measurement errors. The distribution in θ^2_{op} should therefore be approximately gaussian with $dN/d(\theta^2_{op}) \propto \exp(-\theta^2_{op}/2\sigma^2)$. In fig. 9

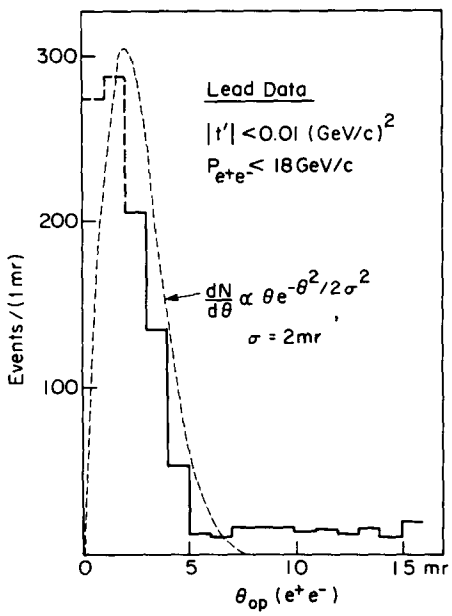

Fig. 9. Opening angle distribution of electron-position pairs in the lead data. The smooth curve shows the expected distribution (arbitrarily normalized) if a Gaussian with a standard deviation of 2 mr is assumed. A standard deviation of $\approx$ 1.6 mr would give a better fit to the data.

the expected distribution for $\sigma = 2$ mr, approximately normalized to the data, is shown. The data indicate that the standard deviation σ is slightly less than 2 mr. The average momentum for the electrons in this sample is 6.7 GeV. Interpolating from table 1, the expected angular resolution $d\theta \approx 1.6$ mr for a single track. The standard deviation in the opening angle θ_{op} is expected to be $\sqrt{2}\,(1.6) = 2.3$ mr, while that observed is less than 2 mr. Thus we believe the calculated resolutions are somewhat conservative.

3.4. Electronics

Fig. 10 shows a schematic diagram of the electronic logic used in this experiment. The trigger requirement was $P_1 L_2 R_2 \bar{A}$ or $P_1 L_3 R_3 \bar{A}$. The blocking gate disabled the electronics for $\approx$ 100 msec after each trigger to permit sufficient time for the spark gaps to recover. It was found that the multiple track efficiency of the chambers deteriorated if the trigger rate was much greater than five triggers per machine pulse. The trigger rate was therefore generally kept at an average of about 4 triggers per pulse.

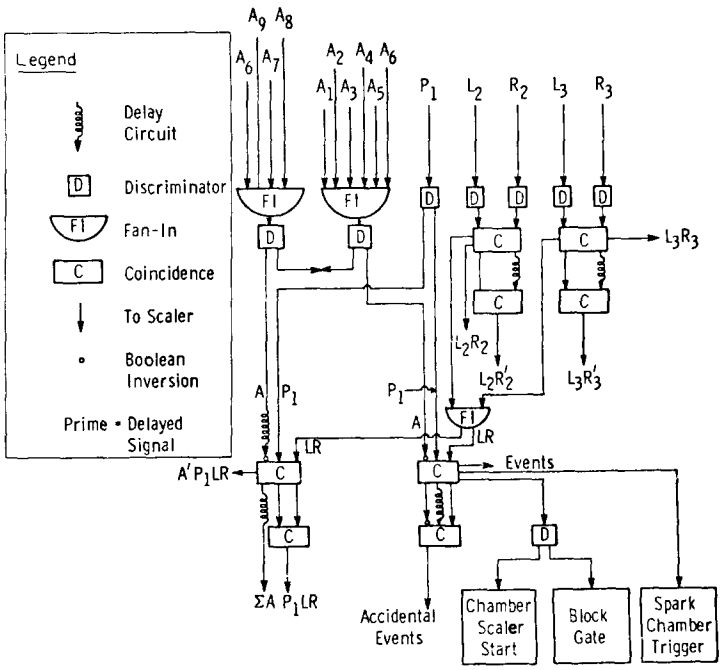

Fig. 10. Electronic logic.

3.5. Operation of the experiment

The data were taken in "runs" lasting several hours with 10 to 20 thousand events per run. Runs were also regularly taken without any target in the target holder. The ratio of the L to M monitor counts was constantly checked to ensure that the neutron beam did not deviate from the nominal beam line. Polaroid film was also exposed in the beam occasionally to check the beam size and position.

The Brookhaven Online Data Facility was used to monitor the performance of the spark chambers during the data accumulation. Data were regularly taken with the spectrometer magnet turned off ("straight-throughs") for checks on the relative spatial positions of the spark chambers. The polarity of the spectrometer magnet was reversed approximately half-way through the data accumulation at the proton beam momentum of 28.5 GeV/c in order to check for any asymmetries in the wire chamber spectrometer. No noticeable difference was found between the data taken before and after the magnet polarity reversal.

4. Data analysis

Since the magnitude of the momentum of the incident neutron and the vector momentum of the recoil nucleus (or its fragments) were not known, the analysis

program could not perform a constrained fit. The kinematics were therefore done with a zero constraint fit which assumed the event came from reaction (1). The angular spread of the beam, estimated to be ± 0.25 mrad, was neglected in the fit. The vector momenta of the proton and the pion were directly measured, and thus the invariant mass $M_{(p\pi^-)}$ of the $(p\pi^-)$ system, the transverse momentum $P_\perp$, and the longitudinal momentum $P_\parallel$ of the $(p\pi^-)$ system could be directly calculated. The $P_\parallel$ of the recoil nucleus was in turn calculated from

$$P_\parallel^{(A)} \simeq (M^2_{(p\pi^-)} - M_n^2)/2P_\parallel \,, \tag{10}$$

where M_n is the rest mass of the neutron. The $P_\perp$ of the recoil nucleus was calculated from momentum conservation, assuming reaction (1). Eq. (10) is correct to within a few percent for this experiment.

4.1. Event reconstruction

The coordinate frame of reference used in the track reconstruction is shown in fig. 11 and the schematic labelling of the wire planes is shown in fig. 12. Since the particles suffered at most small deflections in the vertical direction due to vertical focussing of the spectrometer magnet, and the horizontal bend angles were also generally small, the program initially sought to construct straight line projections of the particle tracks through the wire chamber spectrometer in the vertical plane, i.e., the plane normal to the x-axis. It constructed vertical track projections from all possible combinations of taking one spark in the Y2 plane and one spark in the Y14 plane *.

A vertical track projection was preserved for further analysis only if it had at least two sparks lying on it on each side of the spectrometer magnet, i.e., if it had at least two sparks in each of the sets of wire planes (Y2, Y4, Y6, Y8) and (Y10, Y12, Y14, Y16). The program demanded that a vertical track projection have at least four associated sparks in the horizontal plane, i.e., the plane normal to the y-axis. Two of these

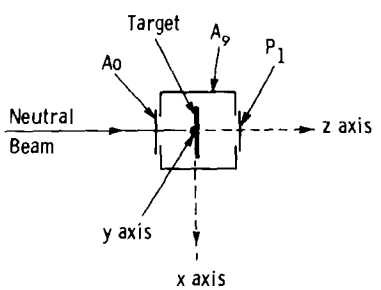

Fig. 11. Coordinate frame of reference for the data analysis.

* Other combinations were also tried, and a change in event yield < 0.5% was found.

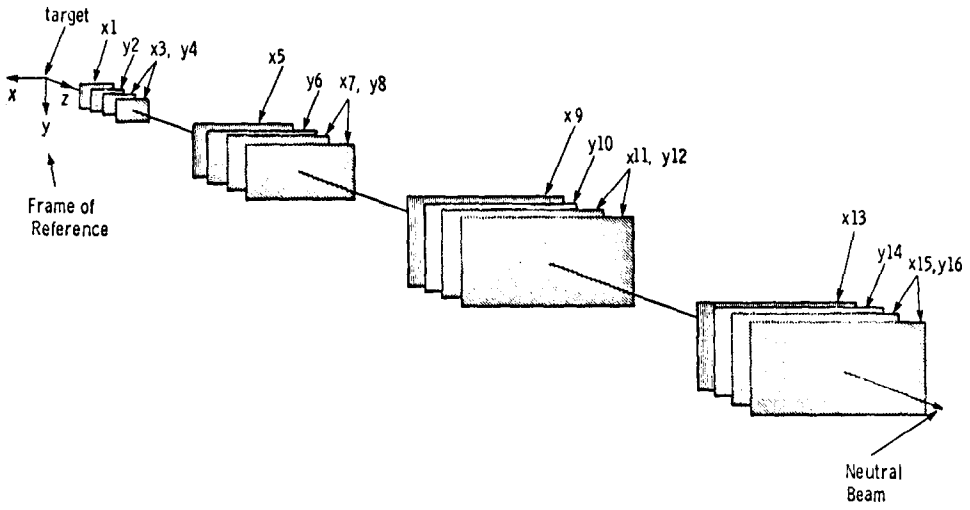

Fig. 12. Schematic labelling of wire planes.

sparks had to be located upstream of the magnet, and two of the sparks downstream of the magnet. The ambiguity of which spark in the horizontal plane ought to be assigned to each spark in the vertical plane, due to the fact that we were detecting two particles in the wire chamber spectrometer, was resolved by the 45° wire planes. The tracks that fulfilled the above spark distribution requirements were kept for further analysis. We call these tracks "event" tracks. According to the above criteria, each event track had to have at least 8 sparks out of the 16 possible.

The event tracks were fitted by the method of least squares. In the fitting process the vertical and horizontal projections of each event track were divided into two "half" tracks, of which one half track lay upstream of the magnet and the other downstream of the magnet. From the least squares fit of each half track to a straight line, each event track was assigned a weight. The two event tracks with opposite bend directions and highest weights that had intercepts at the target in the xy plane less than 2.54 cm from the beam line were assumed to be the proton and pion tracks. A more detailed description of the track reconstruction procedure can be found in ref. [2].

4.2. Event recovery efficiency

A major concern in the experiment was to achieve a high efficiency for events with two (or more) tracks in the spark chambers, magnetostrictive readout, and subsequent analysis. The spectrometer used for this experiment was a modification of that used in an experiment to study np charge exchange scattering [16] in which a single charged particle was detected in the spectrometer. For the diffraction dissociation experiment, the gains of the preamplifiers on the magnetostrictive wands

were turned up considerably, and more care was taken with the gas purity and other aspects of the spark chamber operation. Up to four sparks on each plane could be digitized. However, some difficulty was encountered because of "robbing" of one spark by another. Thus, if there were two or more sparks in one gap, the spark currents tended to be unequal, so that sometimes one of the sparks was not digitized. Another complication was the fact that, in the chambers closest to the target, the proton and pion sparks were often too close together to be resolved and appeared as a single spark. The system, however, was highly redundant; for each track sixteen coordinates were normally digitized while half that number would usually be sufficient to define the trajectory completely.

The track-fitting program was designed to be as efficient in recovering tracks as possible. Table 3 shows the distribution in the number of track projections found in the vertical plane for a sample of about 50 000 event candidates with a carbon target.

An "ideal" event candidate would have two tracks. The large number of 0 and 1 track events reflects the relatively low triggering efficiency of the system (see below). Some of the events with more than two tracks are due to real events with more than two tracks, but most are the result of the looseness of the criteria used for selecting tracks. The proper pairs were sorted out by the weighting procedure described above. Many of the extra tracks were found to differ negligibly from one with a higher weight. These were usually found to be due to a single spark which was digitized twice, either as a result of a small glitch in the shape of the pulse from the magnetostrictive line or a small reflection from the end of the line nearest the pickup coil. Fig. 13 shows the difference between the invariant mass calculated for the best pair of tracks and that for the second best combination. From this and similar evidence, we conclude that the "extra" tracks found did not significantly affect the data.

The efficiency of track reconstruction was checked by loosening the criteria still further. This resulted in a negligible increase in the number of good two-track events recovered ($< 1\%$). Despite the efforts taken to maximize the efficiency of the system, it was found that the variation in the normalized yield of good events from run to run was often considerably outside statistics. Most of the low yield runs were found to have been taken when the chamber gas flow was too low or the chamber system otherwise was not working well. In estimating absolute cross sections it was assumed that the runs with the greatest yields corresponded to essentially 100% efficiency. As a result of this uncertainty in the absolute efficiency, our cross sections could be systematically low; however, the efficiency for recovering

Table 3
Distribution of number of tracks found for a sample of $\approx$ 50 000 event candidates

Number of tracks	0	1	2	3	4	5	6	7	8	≥ 9
Number of "events"	18 115	4 870	11 904	1 141	8 414	166	1 295	148	1 865	533

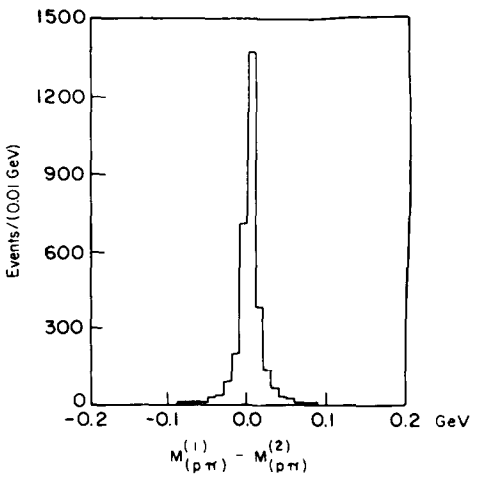

Fig. 13. Difference between best and next-to-best $M_{(p\pi^-)}$.

tracks should be approximately constant for all the targets. It is also unlikely to vary significantly with four-momentum transfer or invariant mass. Tables 4 and 5 list the total number of triggers analyzed for each target and the total number of "good" events (events with at least one positive and one negative track extrapolating back to the illuminated region of the target). The ratio of good events to triggers was $\approx 15\%$ for the data taken with the higher proton energy. This reflects the rather loose triggering requirement which we chose in order to avoid the possibility of introducing unknown biases in the data.

4.3. Target-out correction

To correct for events coming from material other than the target, data were taken periodically with no target in the target holder. The events which survived the analysis program were normalized relative to the monitors and subtracted from the pro-

Table 4
Percentage of good events for the 21 GeV/c data

Target	Carbon	Copper	Target out
Total number of triggers	119 733	63 061	8 367
Total number of good events	11 959	6 572	611
% of total	9.99%	10.42%	7.30%

Table 5
Percentage of good events for the 28.5 GeV/c data

Target	Carbon	Copper	Lead	Target out
Total number of triggers	324 791	164 130	179 690	89 381
Total number of good events	55 308	30 844	24 027	14 999
% of total	17.03%	18.79%	13.37%	16.78%

cessed data taken with the targets in place. The target-out corrections varied from 8 to 58% depending on target thickness.

5. Results

5.1. t' distributions

Figs. 14, 15 and 16 give the t' distributions from carbon, copper, and lead targets for the data accumulated at the proton beam momentum of 28.5 GeV/c, and fig. 17 gives the corresponding distributions for the carbon and copper data taken with a

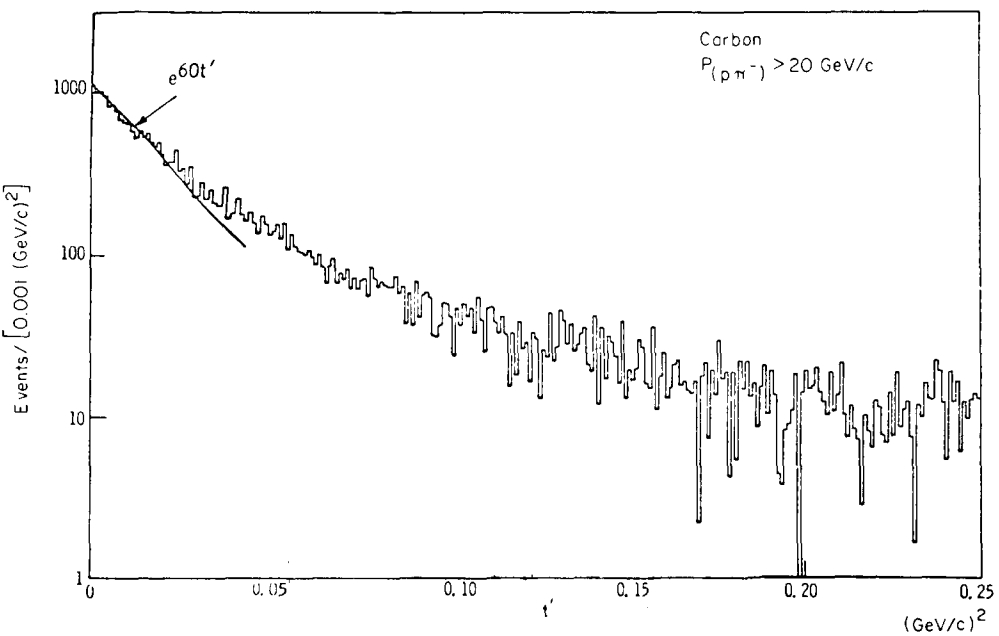

Fig. 14. t' distribution for carbon at the higher proton beam momentum. "Target-out" background has been subtracted. The straight line indicates the expected slope.

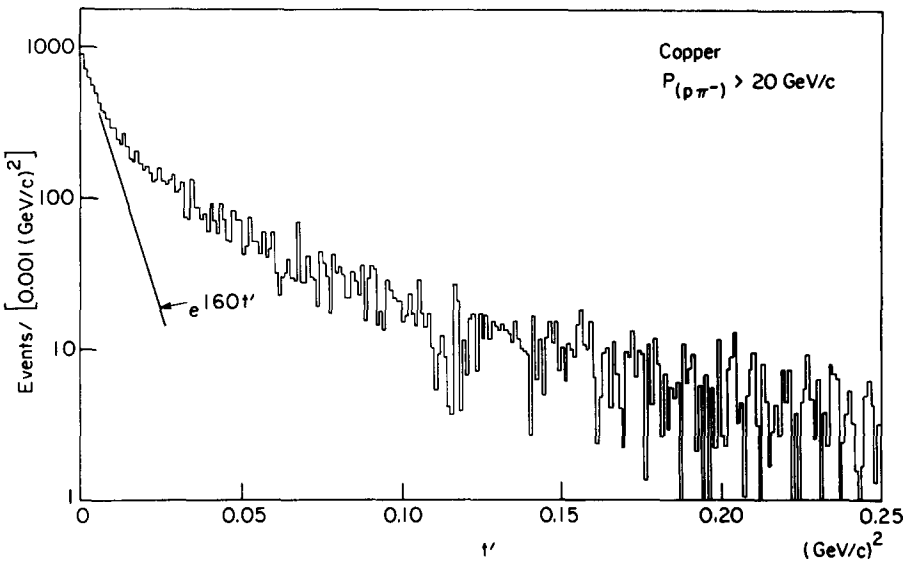

Fig. 15. t' distribution for copper at the higher proton beam momentum. "Target-out" background has been subtracted. The straight line indicates the expected slope.

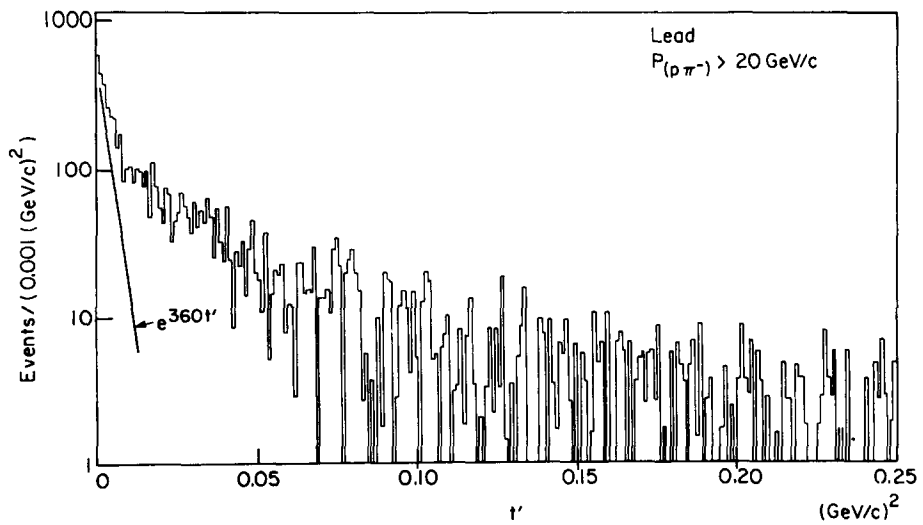

Fig. 16. t' distribution for lead at the higher proton beam momentum. "Target-out" background has been subtracted. The straight line indicates the expected slope.

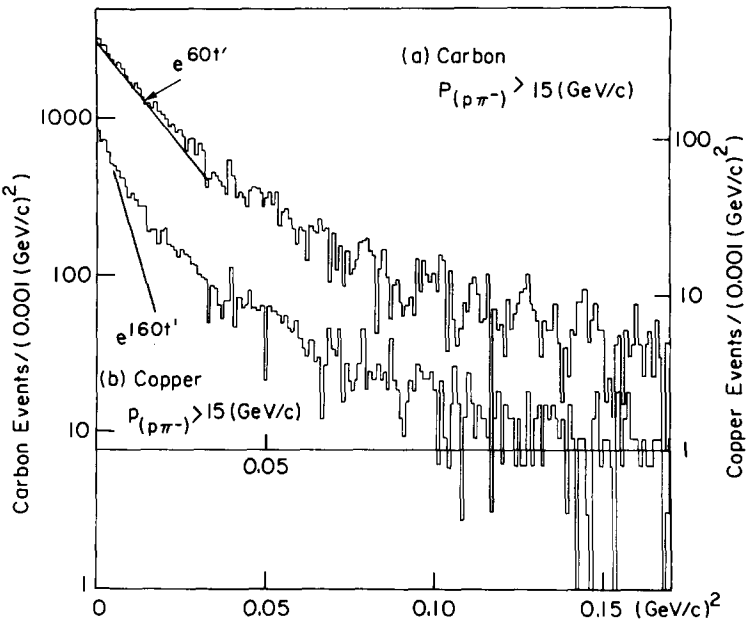

Fig. 17. t' distributions for carbon and copper at the lower proton beam momentum. The right-hand scale is for copper, the left for carbon. "Target-out" background has been subtracted. The straight lines indicate the expected slopes.

21 GeV/c proton beam. In all of these plots, the target-out background has been subtracted. Cuts at 20 GeV/c and 15 GeV/c on the momentum of the ($p\pi^-$) system were applied in these and the figures below to eliminate gamma ray contamination. The sharp forward peaks of width appropriate to the size of the nucleus indicate that the nucleus acted coherently for a large fraction of the events and that at small t' the contamination by processes other than coherent ($p\pi^-$) production is small. A straight line extrapolation indicates that incoherent backgrounds under the coherent peak are $< 30\%$ for $|t'| < 0.02$ (GeV/c)^2 for carbon at the higher proton beam energy, though it is difficult to make a quantitative estimate. The exponential slopes for the coherent peaks are determined by the nuclear radius and are expected to be approximately 60 (GeV/c)$^{-2}$, 160 (GeV/c)$^{-2}$ and 360 (GeV/c)$^{-2}$ for carbon, copper and lead respectively [4]. These slopes are indicated on figs. 14 through 17. The data are generally consistent with the expected slopes if the incoherent background and experimental resolution are taken into account. The events with $-t' \gtrsim 0.05$ have a slope of approximately 10 (GeV/c)$^{-2}$ which suggests they are due principally to incoherent production, n + nucleon $\rightarrow$ ($p\pi^-$) + nucleon. These events also contain some coherent $N + A \rightarrow (p + \pi^- + \pi^0) + A'$, etc. However, the ($p\pi^-$) systems produced off nucleons and from these processes should have a similar t' distribution (where $t' = -P_\perp^2$) since this is typically what one gets for the $P_\perp^2$ distribution for a

single π^0 or nucleon in multiparticle production off nucleons or nuclear targets [3, 15]. Thus coherent production of $\geqslant 3$ particles should have approximately the same $P_\perp^2$ dependence for the two charged tracks as incoherent ($p\pi^-$) production. The bulk of the events in the peak at small $|t'|$ must therefore be coherently produced ($p\pi^-$) pairs, and the background can be estimated by a simple extrapolation of the high $|t'|$ data.

5.2. *Invariant ($p\pi^-$) mass distributions*

The invariant ($p\pi^-$) mass distributions for the higher energy carbon, copper and lead data are shown in figs. 18 through 22, and for the lower energy carbon and copper data in figs. 23 and 24. The target-out background has been subtracted. The

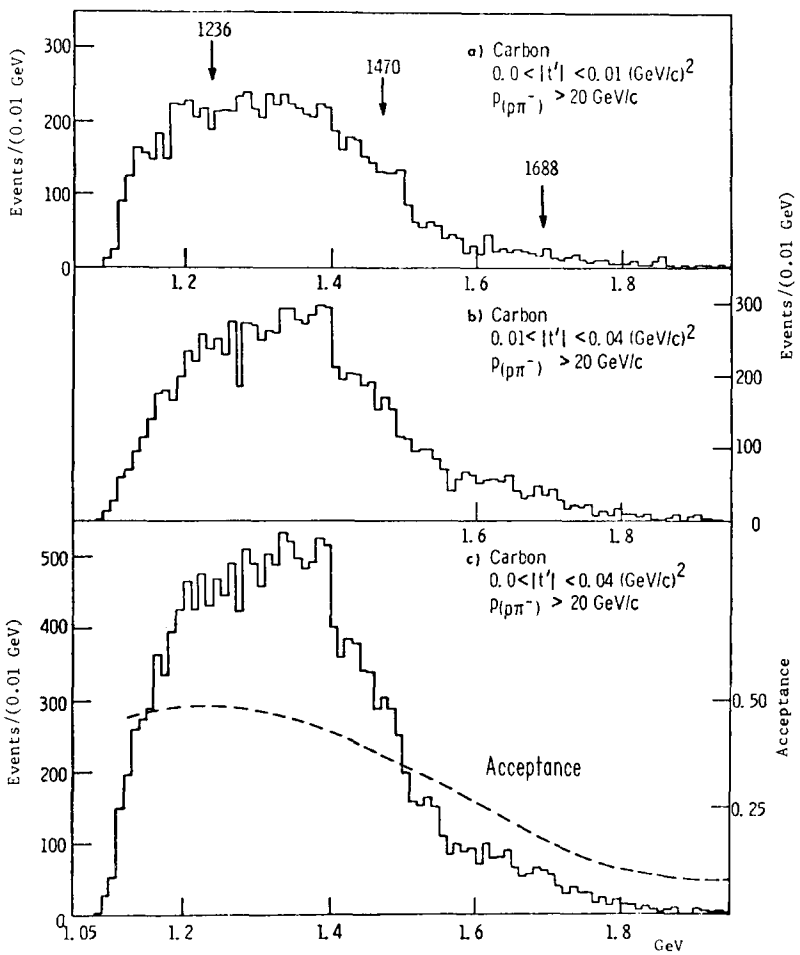

Fig. 18. $M_{(p\pi^-)}$ for carbon at the higher proton beam momentum.

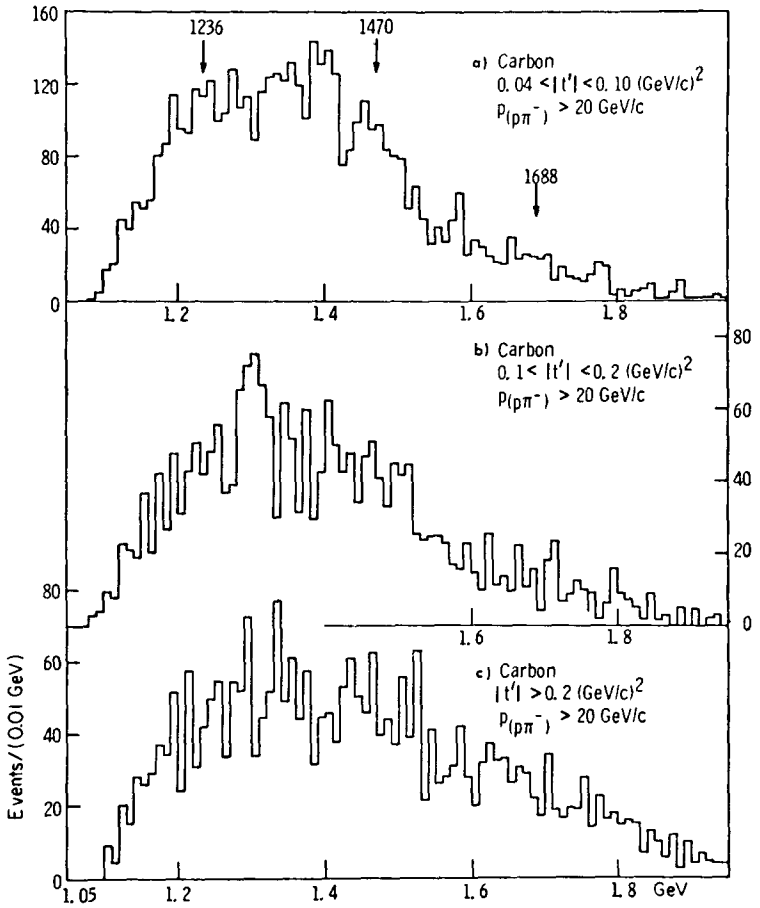

Fig. 19. $M_{(p\pi^-)}$ for carbon at the higher proton beam momentum (cont'd).

data in figs. 18–24 have not been corrected for the geometric acceptance which is shown in fig. 18c. It is estimated that the mass distribution in fig. 18a contains primarily coherent events, the distribution in fig. 18b about 50% coherent events and the distributions in fig. 19, primarily incoherent events. The precise coherent/incoherent ratio for each t' interval is unknown because the state of the recoiling nucleus was not observed and hence an extrapolation of the incoherent t' distribution must be relied upon to indicate the fraction of incoherent events. It can be seen that the mass distributions in fig. 19c, where incoherent production predominates, are broader than the distributions in fig. 18c. There appears to be a general broadening of the mass distribution as $|t'|$ increases*. A similar effect has been noted before [17].

* The high $|t'|$ data also contain an unknown number of events in which additional π^0's or undetected charged particles were produced. This complicates the interpretation of the mass spectra at high $|t'|$.

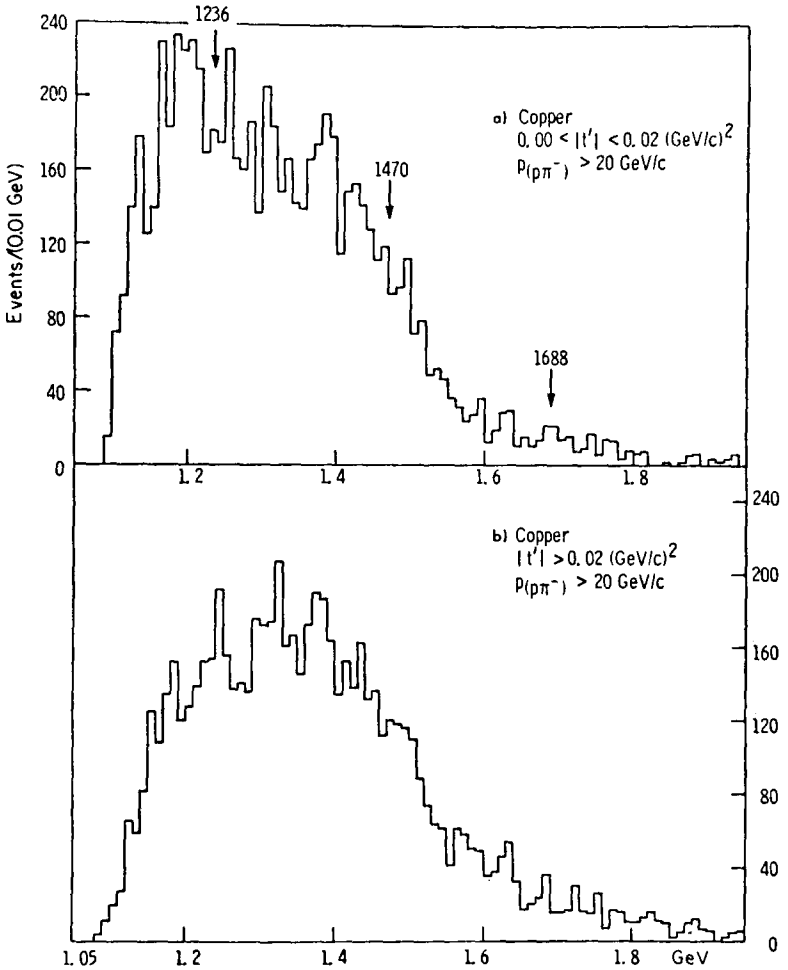

Fig. 20. $M_{(p\pi^-)}$ for copper at the higher proton beam momentum.

The geometric efficiency, which is almost independent of t' over the range studied (see figs. 7 and 18c), was determined from a Monte-Carlo calculation that assumed the θ_π^* distribution is proportional to $(1 + 3\cos^2\theta_\pi^*)$, since this form gives a good fit to the experimentally observed angular distributions [1b]. The fact that the apparatus was insensitive to events with $\theta_\pi{}^* \geqslant 90^\circ$ makes it difficult to estimate the absolute efficiency of the apparatus accurately since the angular distribution outside of the sensitive region of the experiment is unknown (see fig. 6).

The apparent absence of any peaks in the mass distribution corresponding to the well-known N* resonances is perhaps the most striking result of this experiment. From the data in fig. 18c, under the assumption that the background is smooth, we

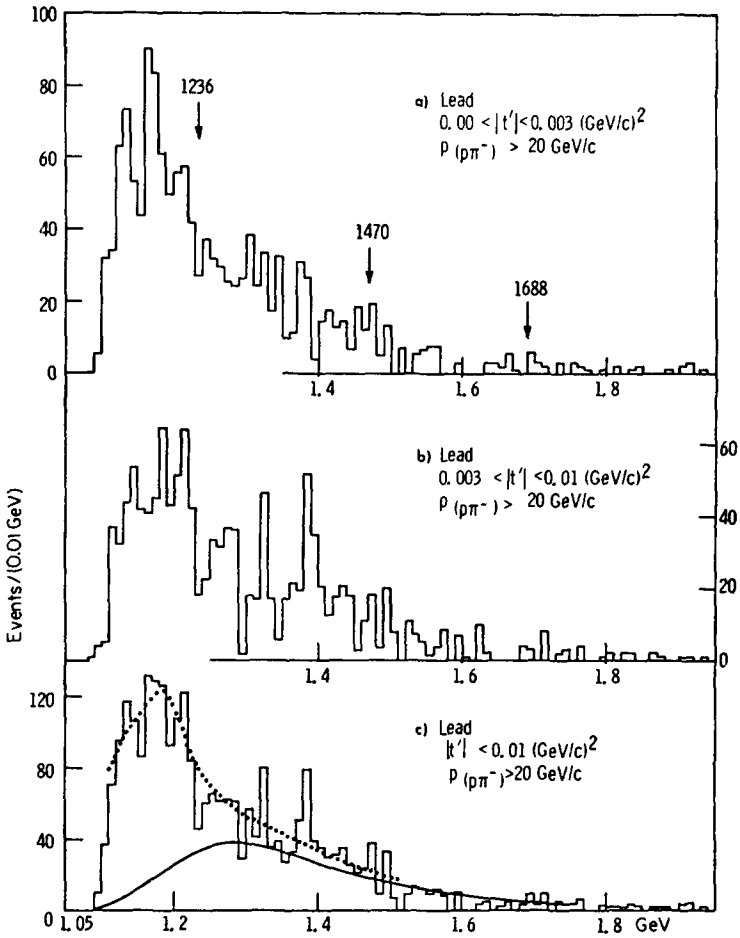

Fig. 21. $M_{(p\pi^-)}$ for lead at the higher proton beam momentum. The dotted curve in (c) is a fit to the mass distribution predicted for coulomb production of the $\Delta(1236)$ with a non-coulomb background indicated by the solid line.

estimate upper limits of 6% and 5% respectively for the N* (1470) and N* (1688) contributions to the total $(p\pi^-)$ events that we see in the region $|t'| < 0.04$ (GeV/c)^2.

The invariant $(p\pi^-)$ mass distributions for the higher energy carbon data for $|t'| < 0.04$ (GeV/c)^2 show little change in shape over the momentum range 15 to 29 GeV/c. This proves that the falloff in the mass spectrum above 1.5 GeV is not due to a nuclear kinematic effect resulting from the increase in $|t_{min}|$ with increasing mass †.

† t_{min} changes from 0.002 to 0.0005 (GeV/c)^2 over this momentum range for $M_{p\pi}$ = 1.5 GeV.

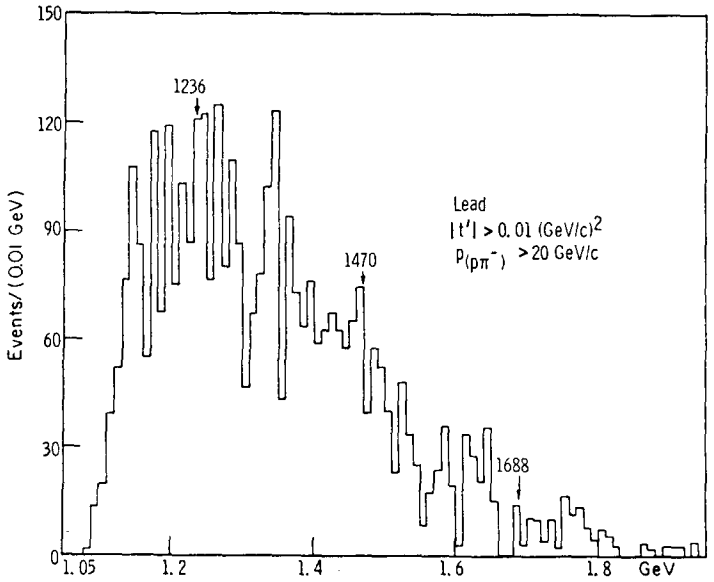

Fig. 22. $M_{(p\pi^-)}$ for lead at the higher proton beam momentum at large t'.

The mass distribution for lead in fig. 21c shows a strong peaking at low mass. If the mass enhancement is the $\Delta(1236)$, which has isotopic spin $\frac{3}{2}$, it could be produced by coherent coulomb dissociation of the incident neutron beam. It is expected that the cross section for coherent coulomb production should possess a steeper t' dependence than diffraction dissociation [5, 10, 18, 19]. Fig. 25 shows the t' distributions for the lead data both inside and outside the Δ mass region *. The lead data for $M_{(p\pi^-)} < 1.23$ GeV, where we have assumed that coulomb dissociation dominates, appears to have a steeper t' dependence than the data for $1.23 < M_{p\pi^-} < 1.4$ GeV **. The rather large incoherent background, however, makes the interpretation difficult. Since the cross section for coulomb dissociation varies approximately as Z^2, it is expected to be small for copper and negligible for carbon. This is observed in figs. 18c, 20a, and 21c.

We have fit the lead data in fig. 21c with the following formula for coulomb production [18]:

$$\frac{d\sigma}{dM_\Delta d|t'|} \simeq \frac{2Z^2\alpha}{\pi}\left(\frac{M_\Delta}{M_\Delta^2 - M_n^2}\right)\frac{-t'}{(t'-t_{min})^2}\sigma_\gamma, \tag{12}$$

* The shape of the $\Delta(1236)$ is badly distorted by dynamic factors and the peak is shifted to approximately 1.18 GeV, as discussed below.

** The width of the peak for $M_{p\pi} < 1.23$ GeV indicates a t' resolution $\approx \pm 0.001(\text{GeV}/c)^2$ for small t'. This provides a check on the calculated t' resolution given in table 2 and an indirect check on the mass resolution.

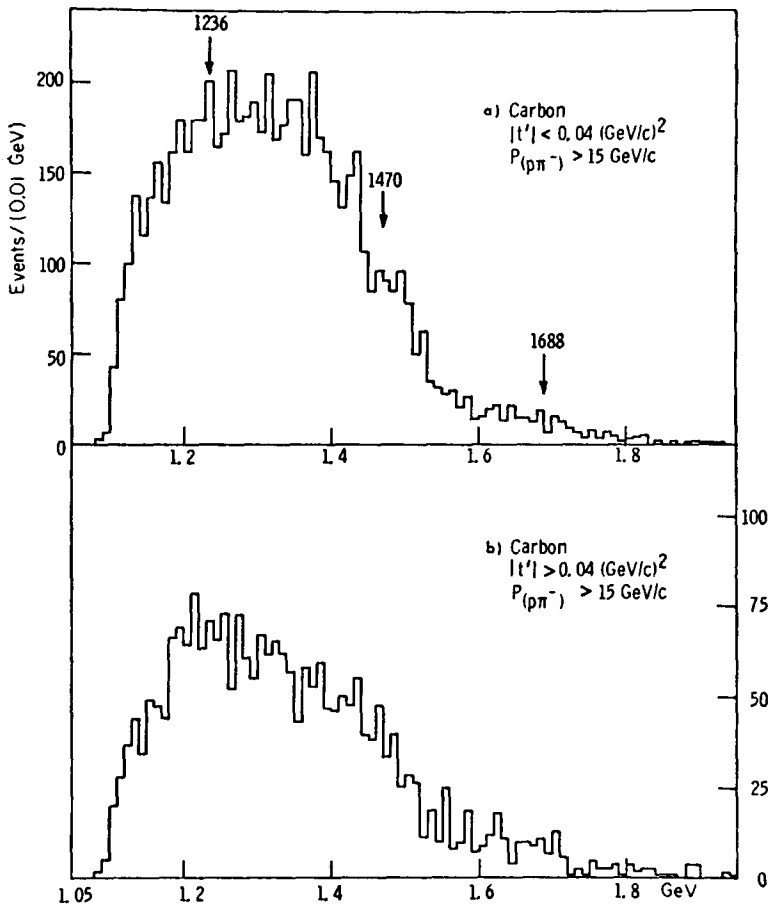

Fig. 23. $M_{(p\pi^-)}$ for carbon at the lower proton beam momentum.

where M_Δ is the invariant mass of the $(p\pi^-)$ system, M_n is the rest mass of the neutron and σ_γ is the experimental photoproduction cross section of the $\Delta(1236)$. This formula agrees with the prediction of Nagashima and Rosen [19] except that we have neglected a term due to the nuclear form factor $F(-t')$, which is very close to unity for the range of t' important in this experiment. In the fit we have assumed that there is a background from diffraction dissociation similar in shape to the observed $(p\pi^-)$ mass distribution for carbon at the higher proton beam energy for $|t'| < 0.01$ (GeV/c)^2. The prediction of eq. (12) was superimposed on the "carbon-like" background and compared with the $(p\pi^-)$ mass distribution for lead after integrating out the t' dependence of eq. (12). We have assumed an effective incident neutron momentum of 25 GeV/c. The values of σ_γ as a function of M_Δ were taken from $\gamma + p \to \Delta^+$ data [20] *. The solid curve in fig. 21c indicates the assumed non-

* The reaction $\gamma + p \to \Delta^+$ is equivalent to $\gamma + n \to \Delta^0$ if there is no $I = 2$ component in the electromagnetic interaction.

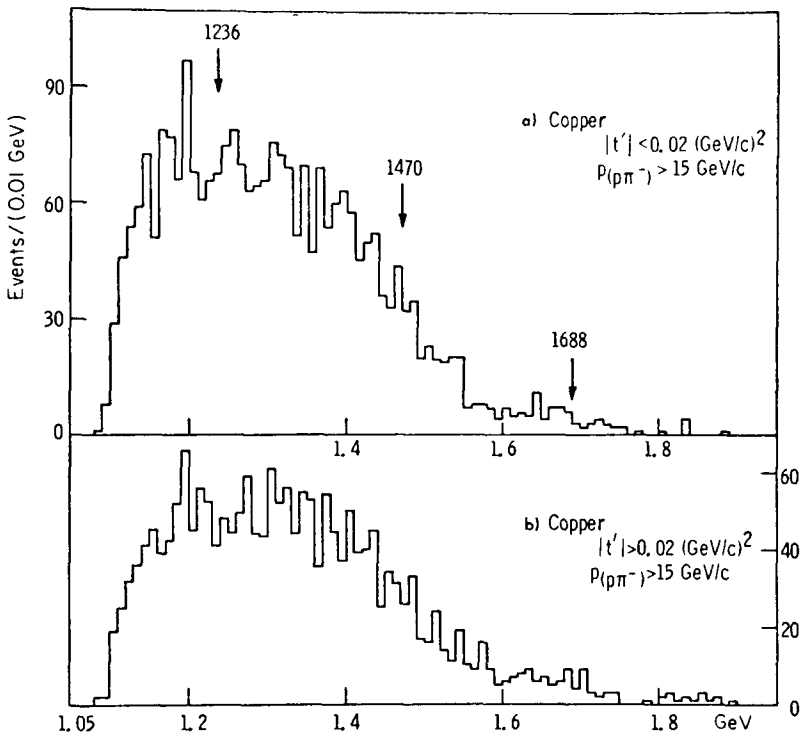

Fig. 24. $M_{(p\pi^-)}$ for copper at the lower proton beam momentum.

coulomb background; the dotted curve shows the expected distribution based on eq. (12) superimposed on the background. The agreement between the observed and calculated curves is excellent. From fig. 21c, we can see that about one-half of the

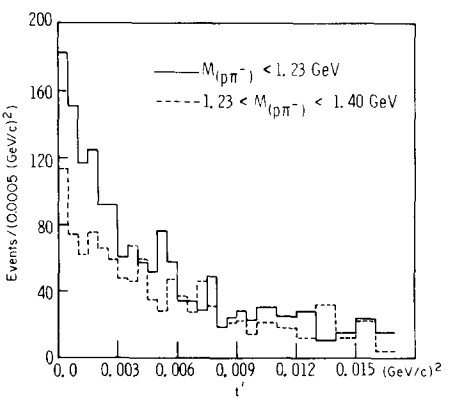

Fig. 25. t' distributions for the lead data for $M_{(p\pi^-)} < 1.23$ GeV and $1.23 < M_{(p\pi^-)} < 1.4$ GeV.

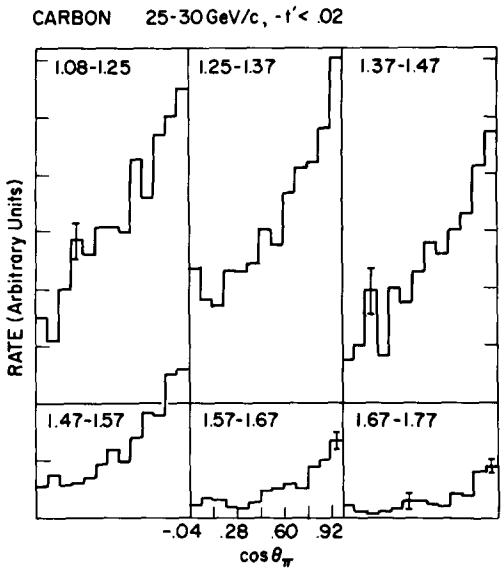

Fig. 26. Cos θ_π in the Gottfried-Jackson frame of reference as a function of $M_{(p\pi-)}$ for carbon at the higher proton beam momentum.

events of the lead data for $|t'| < 0.01$ are due to Coulomb production.

From the lead data we estimate the total cross section for $\Delta(1236)$ production to be 1.6 mb at an effective incident neutron momentum of 25 GeV/c. Nagashima and Rosen [19] predict a total cross section of 1.33 mb for coulomb production of $(p\pi^-)$ pairs by 25 GeV/c neutrons on lead. Due to the uncertainty in the normalization of our data and in the shape of the non-coulomb background, we estimate that our result agrees with their calculation to within a factor of two *.

As pointed out earlier, the mass distributions show no indication of the well-established $I = \frac{1}{2}$ nucleon isobars for t' intervals in the region of the coherent peak. The decay angular distributions, shown in fig. 26, also show no evidence for significant N* production. The target-out background which has a similar shape has not been subtracted since most of it is believed to come from carbon in the counter P_1. The distributions, which have been corrected for detection efficiency, have been cut at $\cos\theta^*_\pi = -0.04$ because the efficiency becomes small beyond this point. These angular distributions show very little change in shape as one moves through the entire mass region, including the region of the known $I = \frac{1}{2}$ nucleon isobars in the interval 1.4 to 1.7 GeV. Essentially the entire coherent cross section appears to arise from a single mechanism which is almost mass independent except for rate. This is

* In a recent experiment, Gobbi et al. [29] have observed Coulomb dissociation of protons into the $\Delta^+(1236)$ in the reaction p + Pb → (p + π^0) + Pb. They also find cross sections in agreement with theory, and, in general, their results agree with ours.

Table 6
Coherent production cross section versus $M_{(p\pi^-)}$ at the higher proton beam momentum

Target	$1.078 < M_{(p\pi^-)} < 1.5$ GeV	$1.4 < M_{(p\pi^-)} < 1.6$ GeV	$1.5 < M_{(p\pi^-)} < 1.8$ GeV
C	1.00 ± 0.27 mb	0.37 ± 0.13 mb	0.23 ± 0.07 mb
Cu	2.27 ± 0.47 mb	0.73 ± 0.19 mb	0.36 ± 0.16 mb
Pb	3.0 ± 1.05 mb	0.63 ± 0.38 mb	0.41 ± 0.29 mb

further evidence against N* production dominating small $|t|$ coherent production of $(p\pi^-)$ systems. The angular distributions for the lower energy data show a similar behavior.

5.3. Cross sections

The coherent cross sections at the higher and lower proton beam energies as a function of invariant $(p\pi^-)$ mass are listed in tables 6 and 7 respectively. The geometrical efficiency of the experimental apparatus (figs. 6, 7, 18c) has been included. For normalization of the cross sections, a total absorption spectrometer [21] in the neutron beam downstream of this experiment was used to determine the number of neutrons per monitor count. We estimate that there is an additional systematic uncertainty of ± 60% in the absolute cross sections. The uncertainty in the absolute cross sections is partly due to fluctuations ~ 40% in the yield of good events/monitor from run to run (subsect. 4.2).

5.4. Spin states, Helicity Conservation, and comparison with models

These results, which have already been discussed in detail in ref. [1b], will be outlined in the conclusions.

5.5. Comparison with other experiments

Several review articles on diffraction and coulomb dissociation experiments have been published [4–7]. This is the first experiment to investigate neutron dissociation into $(p\pi^-)$ pairs off nuclei. Several pp, pd, and $\bar{p}d$ experiments have been done from

Table 7
Coherent production cross section *versus* $M_{(p\pi^-)}$ at the lower proton beam momentum

Target	$1.078 < M_{(p\pi^-)} < 1.5$ GeV	$1.4 < M_{(p\pi^-)} < 1.6$ GeV	$1.5 < M_{(p\pi^-)} < 1.8$ GeV
C	1.12 ± 0.39 mb	0.29 ± 0.08 mb	0.20 ± 0.08 mb
Cu	2.29 ± 0.53 mb	0.59 ± 0.12 mb	0.30 ± 0.08 mb

1.8 to 30 GeV/c to study isobar production. The pp experiments discussed in refs. [3, 22] do not show the characteristic large enhancement we find at low masses in the invariant mass distributions, but rather a series of "resonances" sitting on a large background which generally increases with increasing invariant mass. The background is larger at low incident momenta and appears to be decreasing with increasing incident momentum *.

In order to make a quantitative comparison of our results for a carbon target with the pp results, it is necessary to make some assumptions about the A dependence of the cross sections. We assume that for light nuclei the amplitude at $t = 0$ varies as $A^{0.8}$. Thus we expect

$$\left[\frac{d\sigma(0)}{dt}\right]_{nA} \cong A^{1.6} \left[\frac{d\sigma(0)}{dt}\right]_{pp}.$$

Integrating this expression with the assumption that the cross section falls off exponentially with a slope of approximately $10A^{\frac{2}{3}}(\mathrm{GeV}/c)^{-2}$, we find for the "total" cross section in any mass interval,

$$\sigma_{nA}^{tot} \cong 0.1\ (\mathrm{GeV}/c)^2 A^{0.93} \left[\frac{d\sigma(0)}{dt}\right]_{pp}.$$

We take the N*(1688) as an example. From the data of Edelstein et al. [3], the differential cross section for $p + p \to N^*(1688) + p$ extrapolated to $t' = 0$ is 1.48 ± 0.17 [mb/(GeV/c)^2] at 25 GeV/c. The branching ratio for the decay of the N* (1688) to an (Nπ) system is 60%; two-thirds of these will be (pπ^-) systems if the N*(1688) has $I = \frac{1}{2}$. Thus we would expect for the production of the N*(1688) off carbon with a subsequent decay to pπ^-,

$$\sigma^{tot} \simeq 0.6 \pm 0.07 \text{ mb}$$

from the data of Edelstein et al. [3]. As seen in table 6 and 7 our entire cross section for the mass range $1.5 < M_{p\pi} < 1.8$ GeV is approximately 0.2 mb (with a possible systematic error of ± 60%). Even if half of our events in this mass region (figs. 18c an 23a) could be attributed to N*(1688) production, there is a discrepancy of a factor of at least four **. Possible reasons for this discrepancy are:

(i) a dip in the N*(1688) production for $-t < 0.05$ (GeV/c)^2. The data of Edelstein et al. [3] could easily accommodate such a dip. This possibility has already been discussed by Kane [23].

(ii) an underestimate of the background under the N*(1688) in the pp experiment;

(iii) the bump seen in the pp experiment may not be due to a simple N*(1688) with $I = \frac{1}{2}$ and a 40% branching ratio to pπ^-. (There are at least three $I = \frac{1}{2}$ and two $I = \frac{3}{2}$ resonances reported in this region.)

* These experiments measure the inclusive missing mass distributions. Their background is likely to be quite different from ours. Their peaks also contain all N* decay modes.

** A similar discrepancy occurs for the "N*(1410)".

(iv) a serious error in the normalization of our data. The good agreement between the expected and observed cross sections for coulomb production of the $\Delta(1236)$ on lead would be an argument against this. There is also ample internal evidence that our mass resolution is far better than required to resolve the N*(1688), which has a width of over 100 MeV. However, our experiment was insensitive to decays with $\theta_\pi^* \gtrsim 90°$, and we have effectively assumed a distribution symmetric about 90° in calculating our efficiency. Recent data by Cooper et al., [24] for the reaction $n + p \to (p + \pi^-) + p$ indicate a significant asymmetry with a larger peak near $\theta_\pi^* = 180°$, especially at higher masses *.

The reaction $p + n \to p + p + \pi^-$ has also been studied at 7 GeV/c in a deuterium bubble chamber by Yekutieli et al. [25]. They interpret their data in terms of resonance production with a large background from double Regge exchange, but, in fact, their $(p\pi^-)$ mass distributions and $\cos\theta_\pi^*$ distributions look very similar to ours. Cooper et al. [24] also find mass and $\cos\theta_\pi^*$ distributions very similar to ours in a study of deuterons in a hydrogen bubble chamber at an equivalent neutron momentum of 12.5 GeV/c. Lissauer et al. [17] have also found a very similar mass distribution for $(p\pi^-)$ systems produced by 12 GeV/c K^+ in the reaction $K^+ + n \to K^+ + \pi^- + p$. For $|t'| < 0.08$ (GeV/c)^2, Bastien et al. [26] find a mass distribution like ours for $(p\pi^-)$ states produced by 15 GeV/c π^- on deuterium. Thus there is considerable evidence that resonance production is relatively small for πN systems produced at small t' with incident momenta $\gtrsim 7$ GeV/c.

6. Conclusions

The most striking result of the experiment is the absence of evidence for the coherent production of $I = \frac{1}{2}$ nucleon isobars off nuclei in either the invariant $(p\pi^-)$ mass distributions or the decay angular distributions. Our upper limits for the production of nucleon isobars appear to be inconsistent with a straightforward extrapolation of pp data [3]. There is evidence for coulomb production of the $\Delta(1236)$ in our lead data, but the $\Delta(1236)$ peak is distorted by dynamic factors and is shifted to approximately 1.18 GeV. Aside from the $\Delta(1236)$ in the lead data, the invariant $(p\pi^-)$ mass distributions seem to show a single broad enhancement centered at a mass of about 1300 MeV. Since the decay angular distributions show no significant change between 1100 and 1500 MeV, the enhancement would contain, at best, a small resonant contribution.

For completeness, we will summarize some of the results of ref. [1]. The standard Drell-Hiida-Deck formula [27] does not describe the data for any arbitrary choice of the form factor. Fits by the double-Regge-Pole model are also not completely satisfactory, since the best fits require an umphysical pion intercept of −0.5 (Ref.

* It is important to note that Cooper et al. plot the proton angle while we plot the pion angle. This must be kept in mind when comparing various experiments.

[1b]). The carbon data indicate a spin of the $(p\pi^-)$ system in the low t' region of $J \geqslant \frac{3}{2}$, with pure $J = \frac{3}{2}$ possible. Pure $J = \frac{1}{2}$ can be ruled out for all mass and t' regions. Since we only observe part of the angular decay region, no information concerning the parity of the $(p\pi^-)$ system is available and no definite determination of the spin states of the $(p\pi^-)$ system can be made. No firm conclusions can be drawn from the data concerning s- or t-channel helicity conservation for the coherent events (see ref. [1b]).*.

We would like to thank T.P. McCorriston for writing an online program for the experiment and for his assistance in measuring the neutron beam intensity. We also appreciate the assistance of N. Albers and O. Haas during the setting up and running of the experiment. We especially want to thank L. W. Jones and B.G. Gibbard for their help in various phases of the experiment. The Brookhaven OLDF was used for data acquisition. Helpful conservations with G. Kane are gratefully acknowledged.

References

[1] (a) M.J. Longo et al., Phys. Letters 36B (1971) 560;
(b) J.C. VanderVelde et al., Nucl. Phys. B45 (1972) 1.
[2] D.D. O'Brien, Thesis, University of Michigan report UM HE 72–32, (unpublished).
[3] R. Edelstein et al., Phys. Rev. D5 (1972) 1073;
E.W. Anderson et al., Phys. Rev. Letters 16 (1966) 855.
[4] H.H. Bingham, CERN report D. Ph. II (Phys) 70–60; Proc. of the Topical Seminar on interactions of elementary particles with nuclei, Trieste, 1970.
[5] C.M. Fisher, Methods in subnuclear physics, International School, Herceg-Novi, vol. 1 (1965).
[6] D.W.G.S. Leith, Diffraction dissociation, Proc. of the 16th Int. Conf. on high energy physics, vol. 3 (Chicago, 1972).
[7] D.R.O. Morrison, CERN report D.Ph.II (Phys) 70–64.
[8] M.L. Good and W.D. Walker, Phys. Rev. 120 (1960) 1857.
[9] M.L. Good, CERN report D.Ph.II (Phys) 61–22.
[10] M.L. Good and W.D. Walker, Phys. Rev. 120 (1960) 1855.
[11] K. Gottfried and J.D. Jackson, Nuovo Cimento 33 (1964) 309.
[12] G. Kane, private communication.
[13] F.J. Gilman et al., Phys. Letters 31B (1970) 387;
G. Cohen-Tannoudji et al., Phys. Letters 33B (1970) 183;
R. Silver, California Institute of Technology preprint CALT–68–284.
[14] M.G. Albrow et al., Phys. Letters 33B (1970) 516;
H.W. Hopkins et al., Phys. Rev. Letters 19 (1967) 185;
D. Luers et al., Phys. Rev. 133B (1964) 1276.
[15] J.V. Allaby et al., Contribution to the 4th Int. Conf. on high-energy collisions, Oxford, England, 1972.
[16] M. Davis et al., Phys. Rev. Letters 29 (1972) 139;

* A recent experiment on coherent dissociation of protons off deuterium shows violation of both s- and t-channel helicity conservation [28].

M. Davis, Thesis, Princeton Univ., Elementary particles laboratory report COO–3072–14, September 1972 (unpublished).
[17] D. Lissauer et al., Phys. Rev. D6 (1972) 1852.
[18] L. Stodolsky, Phys. Rev. Letters 26 (1971) 404.
[19] Y. Nagashima and J.L. Rosen, University of Rochester Report UR–875–295, 1969 (unpublished).
[20] G. Källen, Elementary particle physics (Addison-Wesley, Massachusetts, 1964); H.G. Hilpert et al., Nucl. Phys. B8 (1969) 535.
[21] L.W. Jones et al., Phys. Letters 36B (1971) 509; T.P. McCorriston, Thesis, University of Michigan report UM HE 72–11 (unpublished).
[22] K. Fujimura, Prog. Theor. Phys. Suppl. 42 (1967) 282.
[23] G. Kane, Acta Phys. Pol. B3 (1972) 845.
[24] J.W. Cooper et al., University of Michigan preprint UMBC 74–1, submitted to Nucl. Phys.B.
[25] G. Yekutieli et al., Nucl. Phys. B40 (1972) 77.
[26] P.L. Bastien et al., University of Washington preprint VTL PUB–13.
[27] R.T. Deck, Phys. Rev. Letters 13 (1964) 169.
[28] J.W. Chapman et al., Phys. Rev. Letters 30 (1973) 64.
[29] B. Gobbi et al., paper submitted to the 1973 Aix-en-Provence Int. Conf.; J. Rosen, private communication.